P1.87

Tropical and extratropical forecast sensitivity to subtropical observational enhancement

Lee A. Byerle(1), Jan Paegle(2), J.E. Nogués Paegle(2), A. C. Saulo(3), and J. J. Ruiz(3)

(1) USAF, Tucson AZ
(2) Atmospheric Sciences, University of Utah, Salt Lake City, Utah
(3) CIMA/University of Buenos Aires, Argentina

1. Introduction

Two important field projects took place during the past decade over the American continents. Their goal was to improve understanding of warm season processes in sub-tropical regions with monsoonal characteristics. The first (SALLJEX, the South American Low Level Jet Experiment) was executed in the southern summer of 2002-2003, and centered upon Bolivia in South America (see Fig. 1 of Vera et al., 2006). This region was previously a near-data void for operational upper air soundings. Observational deficiencies were substantially reduced during SALLJEX with a significantly enhanced network of atmospheric soundings by radiosondes and pibals (pilot balloons) shown in Fig. 1 (blue squares). Most of the depicted sites were implemented during the experiment, improving the operational observational density during the southern summer of 2003. A second field project (NAME, the North American Monsoon Experiment) took place in northern summer 2004. This project also made additional radiosonde and pibal soundings over a large region, including Mexico, Central America, and portions of the southwestern United States (see Fig. 1 and table 1 of Mo et al, 2007).

Both field programs were primarily motivated by basic research questions regarding atmospheric moisture balances in regions of complex orography within which prior observations were almost completely lacking (South America), or missing during important phases of the hydrological cycle. These phases include, for example, low-level nocturnal jets that occur over both continents. The programs also prompted a series of numerical forecast experiments designed to incorporate the added observations and to evaluate their potential value for short-to-medium range prediction. Many of these experiments used regional models such as the Weather Research and Forecasting (WRF) model (e.g. Ruiz et al., 2010) in an attempt to depict and analyze significant weather events, including severe storms, at resolutions required to resolve heavy precipitation. Others studies, including Mo et al. (2007) and Dirceu et al. (2007) performed global analyses with NCEP (National Centers for Environmental Prediction) analysis tools.

Mo et al. (2007) and Dirceu et al. (2007) assimilated NAME and SALLJEX observations, respectively. Impacts of the analyses on operational climate and forecast models were studied. Figure 2 displays the root mean square (rms) analysis sensitivity to SALLJEX observations (top) and to NAME observations (bottom) for 500-mb winds. These diagrams describe a sub-set of times including every other day in January 2003 for SALLJEX and every other day of July 2004 for the NAME cases. Each experiment lasted more than 2 months, and the NCEP analyses were simultaneously available every 6 h. The samples depicted in Fig. 2 are representative of longer period sensitivity, as described in Dirceu et al. (2007) and Mo et al. (2007).

One striking aspect of the sensitivity to the experimental observations is that impact is not limited merely to the sub-domains within which new observations were made. In both cases, the analysis response spreads throughout the tropical sector around the globe, and continues into the subtropics of each hemisphere. The reasons for the extensive spread of the response are unclear. We speculate that it may be produced by modifications of the first guess fields whose impact propagates around the globe with successive assimilations, and that the analysis impact may become most conspicuous in regions that lack reliable routine observations, including oceanic portions of the tropics. Roads (2003), for example, illustrates the uncertainty in estimating the global tropical hydrologic cycle with reanalyses by comparing NCEP-NCAR and NCEP-DOE (Reanalyses "I and II", respectively) to satellite observations for the years 1998 and 1999. Mo et al. (2007) point out that average, rather than rms wind sensitivity is somewhat more focused in the core region of the NAME experiment, and that rms sensitivity normalized by climate variability is also more constrained to the deep tropics than is the response depicted in Fig. 2, but their measures also show modifications beyond areas immediately adjacent to new observations.

In view of the extensive regions of analysis impact, it is reasonable to use global models to study the forecast response to analysis changes. Mo et al. (2007) performed 4-day predictions with the global CDAS-2 (Climate Data Assimilation System, Version 2) model (Kanamitsu et al., 2002), and found that the rms error was only very slightly improved by the NAME observations, and that the improvement decreased with forecast period. This is not particularly surprising given the remarkable advances in forecast models, observing systems, data assimilation, and analyses tools over the past half century that have taken place independently of special field programs such as SALLJEX and NAME. Many other studies of the influence of regional observational enhancements obtain similarly modest conclusions regarding forecast impacts of localized observation enhancements.

Weissmann and Cardinali (2007), for example, found that regional enhancements of higher latitude observations and analyses over the North Atlantic provide 2-4 day height field predictions by the ECMWF (European Center for Medium Range Forecasts) model with approximately 3% improvement over Europe, but that the impact after 5 days was not significant. Simmons and Hollingsworth (2002) show that over the prior 11 years, the yearly mean reduction of 3-day forecast errors of the ECMWF model of 500-mb geopotential height was only about 1 m for the Northern Hemisphere, and this is also on the order of the few percent improvement noted by Weissmann and Cardinali (2007) in association with regional observation improvement. Although it has proven difficult to demonstrate large forecast improvement with locally enhanced observations, it is sometimes easier to demonstrate forecast sensitivity to initial state changes.

Added observations cannot improve forecasts made by models that are relatively unresponsive to local changes of the initial state. This is the case for some limited area models that often exhibit artificially enhanced predictability because of lateral boundary constraints (Paegle et al., 1997). Miguez-Macho and Paegle (2000, 2001) show that some global models also display relatively small response to locally targeted uncertainties compared to uncertainties of larger scale. Although the SALLJEX and NAME experiments targeted local areas, their analysis impact evidently occurs on much larger scales (Fig. 2). Our present purpose is to study the sensitivity of model forecast changes rather than model forecast accuracy in response to the NAME and SALLEX observations and subsequent analysis impacts.

Section 2 summarizes data sets and models. Section 3 represents a continuation of work presented by Paegle et al. (2007) at the 18th AMS Conference on Numerical Weather Prediction in Park City, Utah. That study discussed a preliminary investigation of forecast sensitivity to the SALLJEX observations in a variety of model configurations. Section 3 repeats some of these experiments for updated models previously used for SALLJEX cases. Section 4 presents similar results for NAME cases. There is now more agreement in the response of the tested models to SALLJEX observations than was the case in our earlier (2007) presentation. Some of the inter-model agreement may correspond to commonality of model biases, similar to problems outlined in the predictability studies of Roman et al. (2004). Model biases can be an important part of forecast error, and the commonality of biases between different models may signal underlying deficiencies that are not yet well-understood. This is addressed in Section 5. Section 6 summarizes conclusions.

2. Data sets and models

Results are taken from five different models. One is a regional implementation of the Weather Research and Forecasting model. Sample forecasts are selected from the NCEP CDAS model, and from reforecasts that incorporate ensembles of NCEP global models. Two research models are also used. The Utah Global Model (UGM) is a primitive equations model, and the global Euler model allows compressibility and non-hydrostatic influences. Initial fields are selected from CDAS-I and CDAS-II analyses, as subsequently described for each experiment.

3. SALLJEX forecast sensitivity

Paegle et al. (2007) studied the response of 5 different model configurations to the presence of SALLJEX observations in the initial state, NCEP (GDAS) analyses. The WRF model was integrated at the University of Buenos Aires Center for Oceanic and Atmospheric Research (CIMA) (e.g., Saulo et al., 2008).

Figure 3 repeats a result presented by Paegle et al. (2007) for the WRF model which was run every 12h for a duration of 48 h during the 3 months of SALLJEX (December 2002 to February 2003). The figure displays the sensitivity of 48-h 500-mb wind predictions defined as the ratio of 48-h rms wind differences between experiments that initially retain and discard SALLJEX observations, divided by initial state differences. The domain for calculations is a sector centered upon South America. During the 48-h forecast, the time-averaged 48-h WRF 500-mb wind sensitivity grows by approximately a factor of 1.1 from the initial time, corresponding to approximately 10% growth of initial state changes after 48 h.

WRF sensitivity (Fig. 3) is slightly stronger than that reported by Paegle et al.'s (2007) simulations of a global primitive equation model (UGM). Those case-averaged UGM integrations showed little forecast sensitivity after 48 h to initial state changes due to SALLJEX observations, in contradiction to results from other tested models. One possible explanation was that the UGM retained more horizontal diffusion than allowed in other models.

More recent experiments confirm this possibility. We repeated a series of 15 day forecasts with the UGM. Forecasts were initialized at 00 UTC starting on 1 January 2003, and every other day thereafter. The model horizontal diffusion was reduced to the smallest amount that allowed stable 2-week integrations. Previously used second order diffusivity, which was specified constant over the globe, was replaced by flow-dependent, fourth-order diffusion. The fourth-order diffusivity is proportional to local horizontal flow gradients and to the meridional grid size squared. Maps shown in Fig. 4 display the forecast evolution of the 500-mb rms wind forecast sensitivity to SALLJEX observations from the initial time through days 4, 9, and 14 of the case-averaged predictions. The forecasts were initialized with two different CDAS-2 global reanalyses (Kanamitsu et al., 2002), which in one case retained SALLJEX observations, and in another case ignored them.

The top left panel of Fig. 4 displays the initial state analysis sensitivity already discussed in Section 1 (see Fig. 2). After 4 days (top right), response to SALLJEX observations begins to appear over North America and the extra-tropical response continues to amplify at day 9 (bottom left) and through 2 weeks (bottom right). After 2 weeks, the strongest response to initial state changes occurs in mid- and high-latitudes of the Northern (winter) Hemisphere.

The opposite (Northern) hemisphere response exceeds that of the Southern Hemisphere after about one week. Area-integrated estimates of the response in Fig. 5 quantify area-integrated sensitivity. The curve with plus (+) signs represents the response calculated in a region centered over South America. Here, the rms response increases from almost 2 m/s to about 2.5 m/s after 2 days; i.e., about 25% amplification over 48 h. This is more than the 48 h amplification of about 10% appearing in the WRF model, and is also substantially stronger than that reported in the UGM experiments described by Paegle et al. (2007). The amplitude of the UGM response is also higher at lower levels (e.g., about 60% at Sigma level 0.84, not shown).

As discussed in the introduction, part of the added initial-state sensitivity with respect to the WRF model may be due to the global UGM domain, while the WRF model used a bounded domain. The extra UGM response relative to our prior UGM integrations may also be due to use of CDAS-2 analyses in the latter (Kanamitsu et al., 2002), rather than the GDAS analyses in Paegle et al.'s (2007) WRF experiments. Furthermore, the present version of the UGM incorporates relatively smaller, and flow-dependent horizontal diffusion, as previously described. The added sensitivity due to the modified horizontal diffusion is displayed in Fig. 6. This diagram shows that enhanced horizontal diffusion is particularly effective to reduce growth of initial state modifications in the winter hemisphere, perhaps because diffusion suppresses uncertainty growth associated with barotropic and baroclinic instability.

This possibility was also discussed by Paegle et al. (2007), who describe a compressible, non-hydrostatic (Euler) model that can be integrated without evident numerical instabilities for 2 weeks in the absence of any explicit horizontal diffusion within the troposphere. The UGM appears to require more horizontal diffusion in order to suppress spectral blocking associated with nonlinear advection terms and use of Fourier transforms.

The response of this Euler model to SALLJEX observations is shown in Figs. 7 and 8. The results are analogous to the UGM reaction to the initial state changes presented in Figs 4 and 5. The Euler model produces substantially stronger reaction to added observations than does the primitive equation UGM in all parts of the globe. In agreement with the latter, the Euler model response maximizes in the Northern (winter) Hemisphere, where it is about twice as great as that found in the primitive equation model.

It is unclear which, if either of the global models represents realistic sensitivity to modification of the initial atmospheric configuration. Figures 9 and 10 present 500-mb anomaly correlations averaged for the 15 cases of the primitive equation UGM and the global Euler models, respectively. The differences are slight, with the Euler model showing somewhat higher skill (e.g. a correlation coefficient of 0.6 or greater), possibly because of its smaller diffusion. The difference could also be explained by different treatment of radiative processes in the two models, which will be discussed in the conclusion (Section 6).

Both the UGM and the Euler models show significantly less skill than the GFS reforecast system (Hamill et al., 2004), whose results are depicted in Fig 11 for the same 15 days, also initialized at 00 UTC, using the ensemble average. Globally computed anomaly correlations in excess of 0.6 occur slightly beyond 6 days of prediction in the reforecasts, approximately one day longer than the UGM and Euler model results of Figs. 9 and 10, respectively.

The reforecast model framework (Hamill et al., 2004) consists of ensembles of forecasts for each case that are initialized with different estimates of the initial state. Initial fields are from the NCEP-NCAR Reanalysis, Version 1 (Kalnay et al., 1996; Kistler et al., 2001). Seven pairs of perturbed reanalysis conditions provided by the "breeding method" and a control member (15 members, total) are used to initialize a previously operational version of the NCEP GFS model (operational January-June 1998) truncated at wave number 62. This represents slightly better resolution than that used in the UGM and Euler models where the longitude structure is truncated at wave number 42. The next sections (4 and 5) suggest that the ensemble approach also provides major benefit for the reforecast model, and demonstrates that our research models may provide useful guidance to investigate forecast problems that appear to be common to both ensemble and single forecast methods.

4. NAME forecast sensitivity

Initial state sensitivity experiments were repeated for versions of the global Euler model initialized with CDAS 2 reanalyses with and without NAME observations. The initial analyses were kindly provided by Dr. Kingtse Mo, who also supplied 4-day predictions of the CDAS forecast model for present experiments. The analyses are used here to start the Euler model in 15 day predictions initiated every other day beginning at 00 UTC on 1 July 2004. As in the SALLJEX integrations of the previous section, the model was run for 15 cases, and all results are averaged over these events.

Figure 12 depicts time evolution of 500-mb rms wind forecast differences produced by the Euler model initiated from different states that included or denied NAME observations. Similar to the SALLJEX cases, the impact of NAME observations propagates toward mid-latitudes of both hemispheres on a time scale of a week and continues to amplify through the period of prediction. Area-averaged sensitivity is displayed in Fig. 13, and the results are similar to those presented in Fig. 8, with maximum response in the opposite, Southern (winter) Hemisphere. The responses possess similar amplitude to SALLJEX cases (compare to Fig. 8).

We next compare anomaly correlations produced by the global Euler model forecasts (Fig. 14) with those from the reforecasts (Fig. 15) incorporating ensemble forecasts for the same cases, and with CDAS predictions provided by Dr. Mo (Fig. 16). The selected cases start at 00 UTC every other day of July 2004, beginning 1 July. Figure 14 shows anomaly correlations of forecasts by the global Euler model for the NAME cases. Globally-averaged cases have anomaly correlations exceeding 0.6 for almost 6 days. By contrast, globally-averaged anomaly correlations for the same 15 cases by the reforecasts exceed 0.6 for about 7 days, or approximately one day longer than does our Euler model (Fig. 15).

As described above, the GFS reforecasts are produced by a version of the GFS that is initialized by an ensemble of 15 different estimates of the initial state, each of which represents a perturbation of the best estimate of the initial state provided by the "breeding method" (Hamill et al., 2004) and is then projected into the future by the GFS prediction model. On the other hand, the present Euler model experiments consist of a single realization for each case that is based upon the single analysis for that case provided by the CDAS 2 analysis system (Kanamitsu et al., 2002). This approach is similar to one taken by Mo et al. (2004) within which single CDAS 2 analyses with and without NAME observations are used to initialize the CDAS forecast model.

Mo et al. (2007) produced 96 h forecasts with the CDAS forecast model. The anomaly correlations of the resulting predictions that retained NAME observations in the initial state are depicted in Fig. 16. After 96 h, anomaly correlations are slightly less than 0.8 in each hemisphere, as well as on a global basis. Figure 17 displays anomaly correlations averaged over the same 15 cases for predictions produced by the global Euler model used in our research. The small differences with Mo et al.'s (2007) anomaly correlations from the CDAS model are depicted in Fig. 18.

There is a substantial high-frequency oscillation in our global Euler model that is especially notable in the Northern (summer) Hemisphere (Fig. 18). This is likely due to lack of dynamical balancing within the initial state of the Euler model. The initial conditions of the Euler model are taken from linear spatial interpolation of analyses provided by the CDAS 2 data set to our model grid. Although this data set probably includes reasonably well-balanced states for primitive equation models, there is no guarantee that these fields are well-balanced for non-hydrostatic, compressible models such as the Euler model incorporated on our present grid. It is also possible that resulting imbalances contribute to the forecast sensitivity displayed by the Euler model to the presence or absence of NAME and SALLJEX observations.

Although the Euler model may contain significant initial state imbalances, its predictions have similar accuracy as those provided by the CDAS model.

5. Model biases

One advantage, and possibly the most important benefit of the reforecast approach, is its use of ensemble methods, which provide many forecasts for each case that are subsequently averaged. This requires more computer resources than does a single forecast for a single case. Another way to improve forecast accuracy is to increase the model resolution. This requires more compute effort but provides more accuracy, as shown by Roman et al. (2004) and many others.

Roman et al. (2004) compared the high resolution operational NCEP GFS forecasts with lower resolution predictions of the presently used UGM model and determined that, although the higher resolution operational model is substantially more accurate, its error configurations correlate with those of the UGM. Furthermore, this correlation exceeds that which may be expected from purely random evolution associated with the sensitivity of a chaotic forecast system from uncertain initial states.

These issues motivate the results of the present section. Figure 19 presents anomaly correlation of the Euler model forecasts with respect to GFS reforecast model predictions rather than analyses. For the Southern (winter) Hemisphere (open circles) within which each model displays the greatest skill, the models predict each other's behavior more accurately than either predicts the actual evolution. The Southern Hemisphere forecasts by the GFS reforecast model of the Euler model forecast possesses about 24 h longer 500-mb skill at an anomaly correlation of 0.6 than does its prediction of the actual evolution. Likewise, the Euler model skill in predicting the GFS reforecast model at this accuracy level carries about 48 h more validity than does its prediction of actual conditions. These conclusions can be derived by comparing Fig. 19 with Figs 14 and 15, and noting that the model-to-model forecast anomaly correlation in the Southern Hemisphere is higher than are either of the model anomaly correlations with the evolving weather.

One reason for the inter-model forecast similarity is the similarity of model biases. Figures 20 and 21 show the 15-case averaged, meridional, 500-mb geostrophic wind biases for 360 h predictions provided by the reforecast and by the presently used Euler research model, respectively. Much similarity is evident in many regions. In particular, both models display negative biases over the east coast of North America, positive biases over the Rocky Mountains, and negative biases over the Gulf of Alaska. It is easy to identify similarities in many other areas. The globally calculated correlation coefficient between the patterns of these two figures is almost 0.7, and it is close to 0.8 in the Southern Hemisphere.

Figure 22 presents time evolution of correlations of meridional wind biases of the Euler model with meridional wind biases of the reforecast model. Roman et al. (2004) argue that these correlations should asymptote to 0.5 for purely chaotic and random events. In the present July 2004 case, as in the one presented by Roman et al. (2004) in which biases of NCEP operational model predictions were correlated with those of experimental UGM predictions during January-February 2003, the bias correlations increase with forecast duration, and eventually exceed 0.5, globally, and in each hemisphere. We conclude that the errors of the presently studied primitive equation models and of the Euler models are not controlled only by purely chaotic processes, but also contain systematic, and potentially removable, components.

6. Conclusions

This study is motivated by basic research questions that arose in earlier work emphasizing the value of new observations in the SALLJEX field program, and the degree to which forecast sensitivity to the added data depends upon model configuration. The basis of the prior conclusions has now been extended to include initial states provided from the NAME field program, and added ensemble ("reforecast") versions of the GFS model as well as single realization predictions of the CDAS model and the UGM and global Euler models used in our prior related studies.

Consistent with Paegle et al. (2007), we find that the analysis enhancements provided by field experiments executed in the summer sub-tropics provide important initial state modifications throughout the tropical belt. The forecast impact spreads into higher latitudes on a time scale of approximately one week, and continues to amplify through two weeks. The strongest effect is by then noted in the opposite winter hemisphere. The amount of horizontal diffusion retained in the models exerts important controls upon the response to the added data, as does the effect of using limited area or global models.

The global primitive equation model we used in prior research has been modified to run with smaller amounts of horizontal diffusion, allowing significantly enhanced responses to changed initial states. Nevertheless, the Euler model used here displays approximately twice as great a response to changes of the initial state as does the UGM. This is probably due to the fact that this model does not include explicit horizontal diffusion below 14 km.

In addition to the dynamical cores, and diffusion treatment, the Euler model and the UGM have different treatments of atmospheric radiation processes. To save computer time, the Euler model imposed radiative heating fields within the atmosphere that are taken from NCEP-NCAR Reanalysis climatology. Roman et al. (2004) report that specifying such climatological radiation heating in the UGM provided predictions that are very similar to those emerging from model runs using internally calculated radiative heating everywhere. While the approach should not contribute to greater forecast sensitivity in the Euler model, it may contribute to the slightly higher accuracy of that model relative to the UGM, since the reanalysis climatology is likely to be well-tuned to the actual atmosphere.

One of the most important findings is the remarkable, and growing correlation, between the biases of different models and of the resulting model similarities. Roman et al. (2004) pointed out similar results in comparing the high-resolution, operational GFS and lower resolution, research UGM. We have now demonstrated similarly high correlations between the research Euler model and climate models executed in ensemble predictions from real initial states. The reasons for the large model-to-model error similarities are not clear and merit further study.

Acknowledgments. NOAA Grant NA06AR4310048; SALLJEX was funded by NOAA/OGP, NSF(ATM0106776) and funding agencies from Brazil FAPESP (Grant 01/13816-1) and Argentina (ANPCYT PICT 07-06671, UBACyT 055). GFS reforecast data was kindly provided by NOAA ESRL, Physical Sciences Division. Dr Kingtse Mo of NCEP kindly provided the NAME analyses. Contact: lee.byerle@dm.af.mil .

7. References

Dirceu, H., V. E. Kousky, and W. Ebisuzaki, 2007: The impact of high-resolution SALLJEX data on NCEP global analysis. *J. Climate*, 20, 5765.

Hamill, T. M.,J. S. Whitaker, and X. Wei, 2004: Ensemble re-forecasting: Improving medium-range forecast skill using retrospective forecasts. *Mon. Wea. Rev.,* 132, 1434-1447.

Kalnay, E., and Coauthors, 1996: The NCEP/NCAR 40-year Reanalysis project. *Bull. Amer. Meteor. Soc.*, 77, 437-471.

Kanamitsu, M., W. Ebisuzaki, J. Woolen, S-K. Yang, J. Hnilo, M. Fiorino, and G. L. Potter, 2002: NCEP-DOE AMIP-II reanalysis(R-2). *Bull. Amer. Meteor. Soc.*, 83, 1631-1643.

Kistler, R. and Coauthors, 2001: The NCEP-NCAR 50-Year Reanalysis: Monthly means CD-ROM and documentation. *Bull. Amer. Meteor. Soc*., 82, 247-268.

Miguez-Macho, G. and J. Paegle, 2000: Sensitivity of a global forecast model to initializations with reanalysis data sets. *Mon. Wea. Rev*., 128, 3879-3889.

Mo, K., E. Rogers, W. Ebisuzaki, and R. W. Higgins, 2007: Influence of the North American Monsoon Experiment (NAME) 2004 enhanced soundings on NCEP operational analyses. *J. Climate*, 20, 1821-1842.

Miguez-Macho, G. and J. Paegle, 2001: Sensitivity of a global forecast model to initializations with reanalysis data sets. *Mon. Wea. Rev.,* 128, 3879-3889.

Paegle, J., 1989: A variable resolution global model based upon Fourier and finite-element representation. *Mon. Wea. Rev*., 117, 583-606.

Paegle, J., L. A. Byerle, J. Ruiz, A. C. Saulo, and J. N. Nogués Paegle, 2007: Sensitivity testing of a new model with special observations. Preprints from the 18th Conference on Numerical Weather Prediction, Park City, UT. Available at http://ams.confex.com/ams/pdfpapers/123418.pdf.

Paegle, J., Q. Yang, and M. Wang, 1997: Predictability in limited area and global models. *Meteorol. Atmos. Phys.*, 63, 53-69.

Roads, J., 2003: The NCEP-NCAR, NCEP-DOE, and TRMM tropical atmosphere hydrologic cycles. *J. Hydrometeor*., 4, 826-840.

Roman, J. C., G. Miguez-Macho, L. A. Byerle, and J. Paegle, 2004: Intercomparison of global research and operational forecasts. *Wea. Fcsting*, 19, 534-551.

Ruiz, J. J., C. Saulo, and J.N. Nogués Paegle, 2010: WRF model sensitivity to choice of parametrization over South America: validation against surface variables. *Mon. Wea. Rev*., doi: 10.1175/2010MWR3358.1, in press.

Saulo , A. C., S. Cardazzo, J. Ruiz, C. Campetella and A. Rolla, 2008: Experimental forecast system at the Research Center for the Sea and the Atmosphere. *Meteorologica*, 33, 83-97.

Simmons, A. J. and A. Hollingsworth, 2002: Some aspects of the improvement in skill of numerical weather prediction. *Q. J. R. Meteorol. Soc*, 128, 647-677.

Vera, C., J. Baez, M. Douglas, C. B. Emanuel, J. Marengo, J. Meitin, M. Nicolini, J. Nogués Paegle, J. Paegle, O. Penalba, P. Salio, C. Saulo, M. A. Silva Dias, and E. Zipser, 2006: The South American low-level jet experiment. *Bull. Amer. Meteor. Soc*., 87, 63-77.

Weissmann, M., and C. Cardinali, 2007: Impact of airborne Doppler lidar observations on ECMWF forecasts. *Q. J. R. Meteorol. Soc*., 133, 107-116.

Figures:

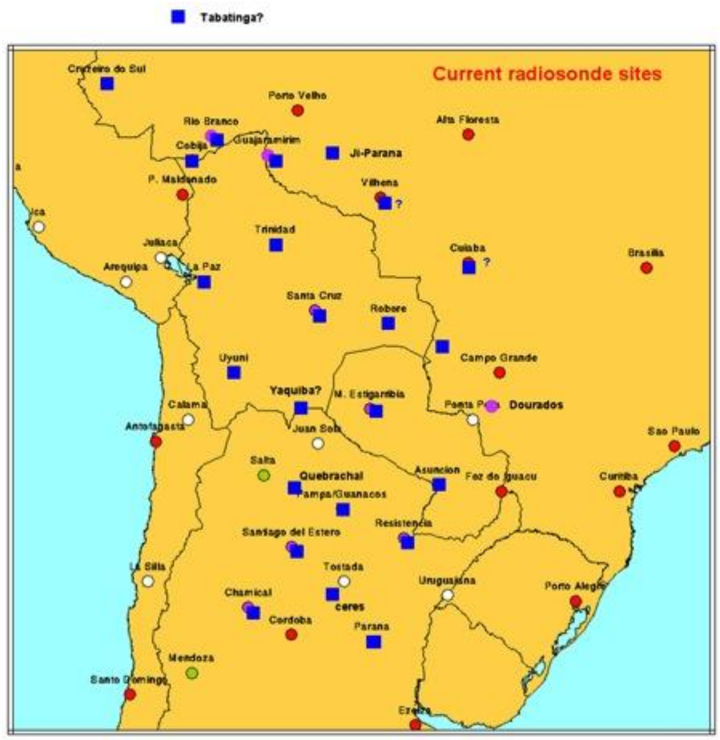

Fig. 1 South American observational deficiencies were partly corrected during the Southern summer of 2003 by the SALLJEX field program. The blue dots show locations of added upper-air wind observations (Vera et al., 2006).

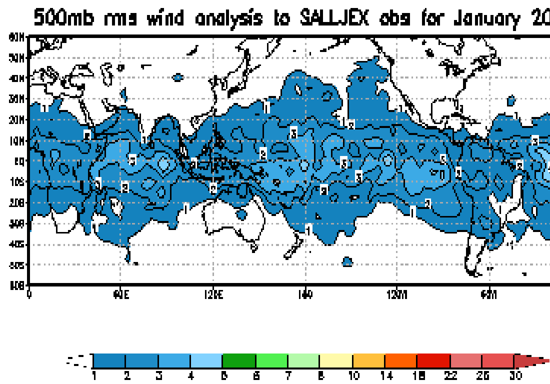

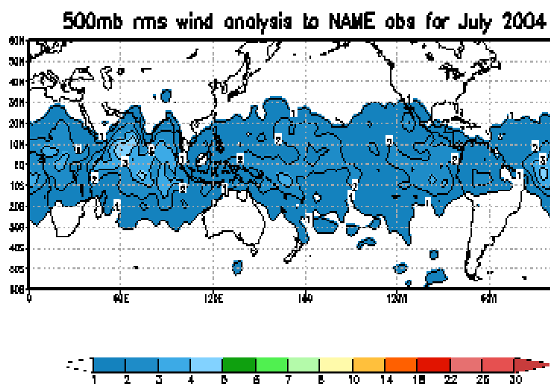

Fig. 2 Root-mean-square (rms) analysis sensitivity to SALLJEX (top) and NAME observations(bottom) for 500-mb winds, averaged for every other day of January 2003 (top) and July 2004 (bottom), beginning the first day of each month, at 00 UTC.

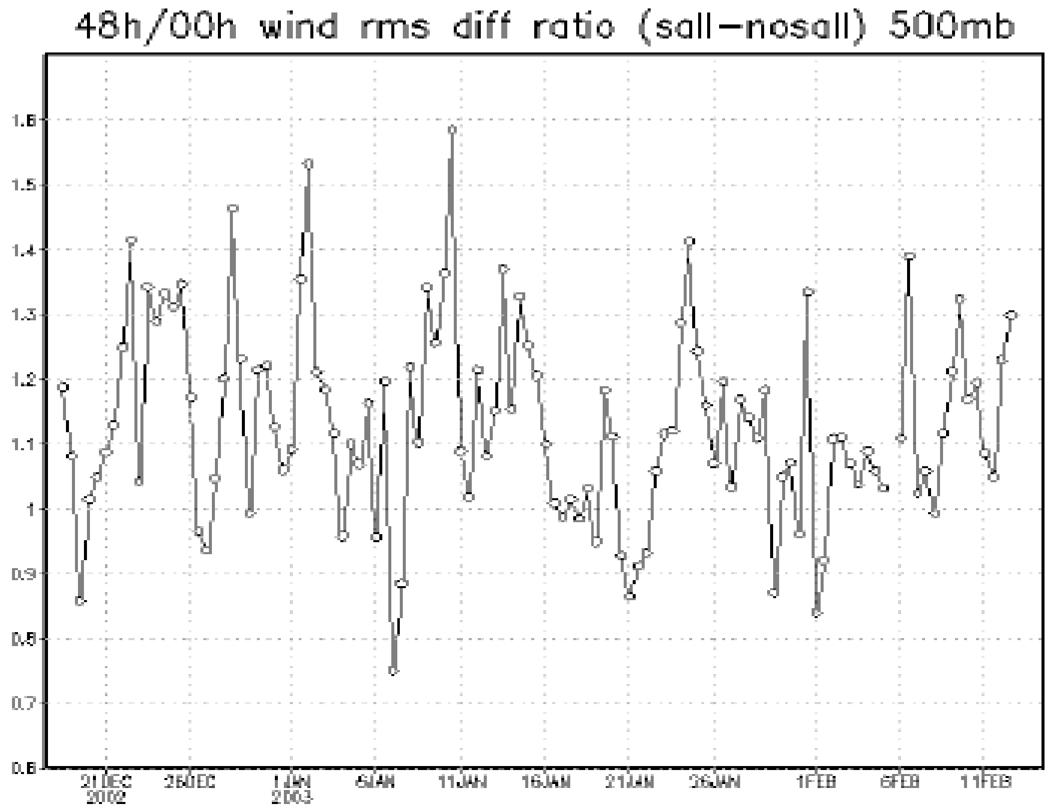

Fig. 3 Time series, from late December 2002 to mid-February 2003, of 48-h WRF model forecast 500-mb rms wind difference (m/s) between the control forecasts and the experimental forecast at 48 h divided by initial value within 50S-Eq, and 100W-30W (South America). From Paegle et al. (2007).

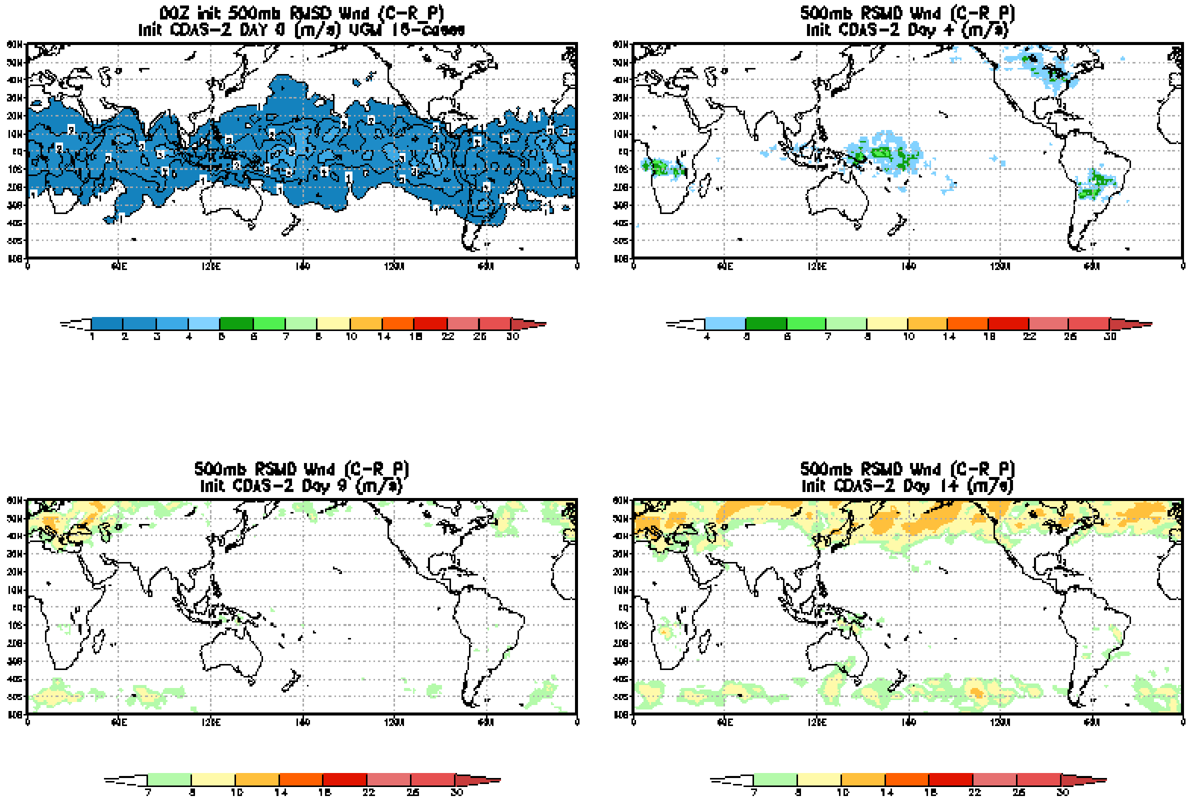

Fig. 4 RMS difference (m/s) between 500-mb wind forecasts made by the Utah primitive equation global model (UGM) with and without SALLJEX observations. Day 1 (upper left), day 4 (upper right), day 9 (lower left), and day 14 (lower right) forecast times are displayed. 15-case averages are shown for integrations initialized every other day in January 2003, starting 1 January.

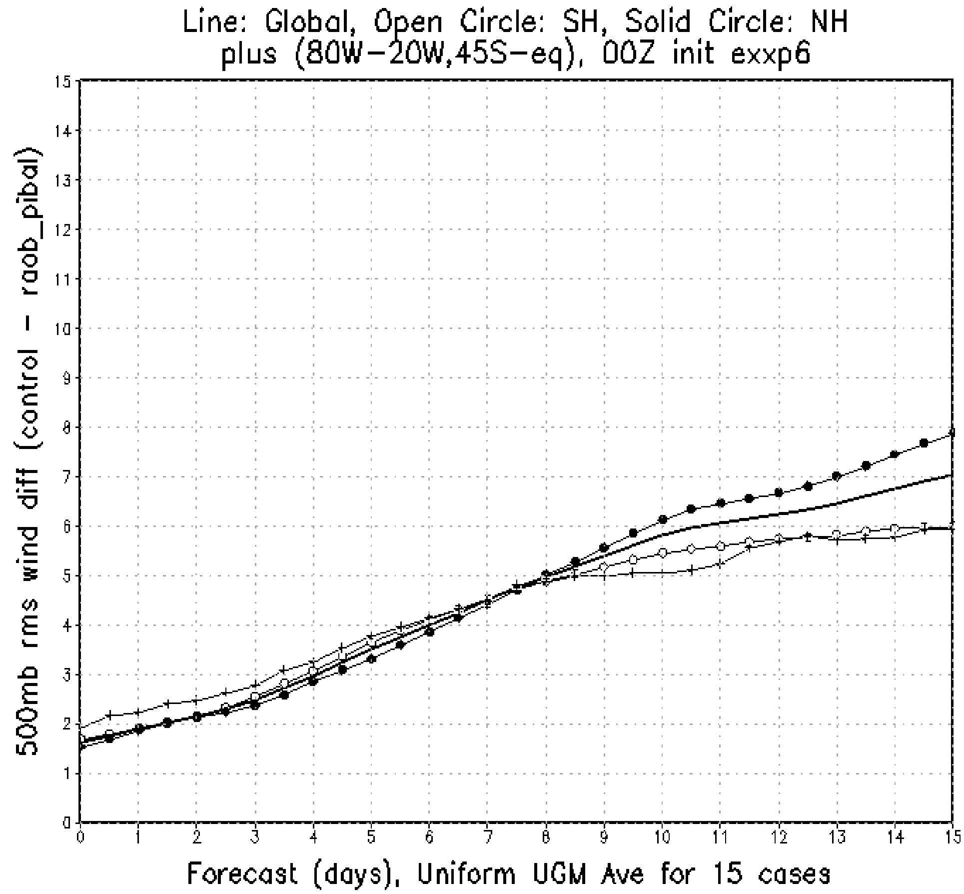

Fig. 5 Time evolution of area integrated rms sensitivity between 500-mb wind forecasts made by the UGM using initial states (00 UTC) with and without SALLJEX observations. The solid line represents globally-averaged sensitivity; solid circles Northern Hemisphere; open circles Southern Hemisphere; and the line with plus (+) signs represents an average over a domain centered on South America from 80W-20W, 45S-Eq.

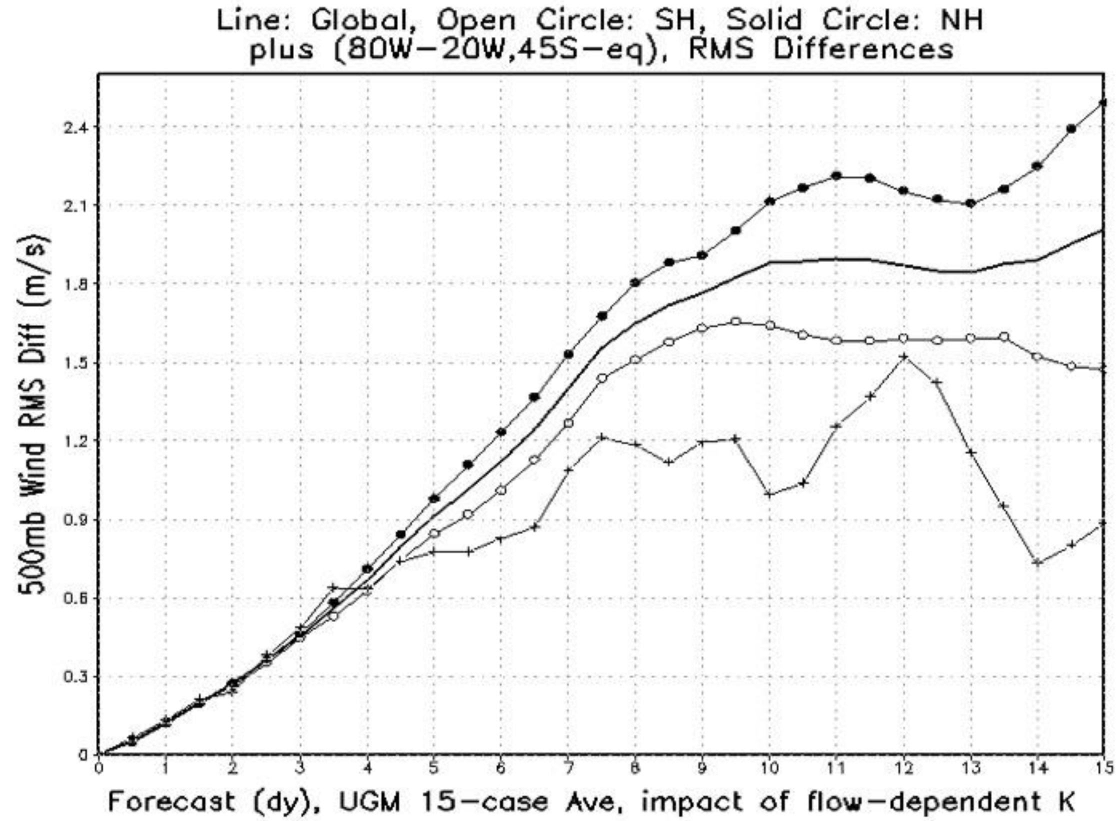

Fig. 6 As in Fig. 5, but for area-integrated difference in sensitivity to SALLJEX observations between UGM simulations (06 UTC initialization) that retain constant horizontal diffusion and those in which horizontal diffusion is reduced and is proportional to local wind gradients.

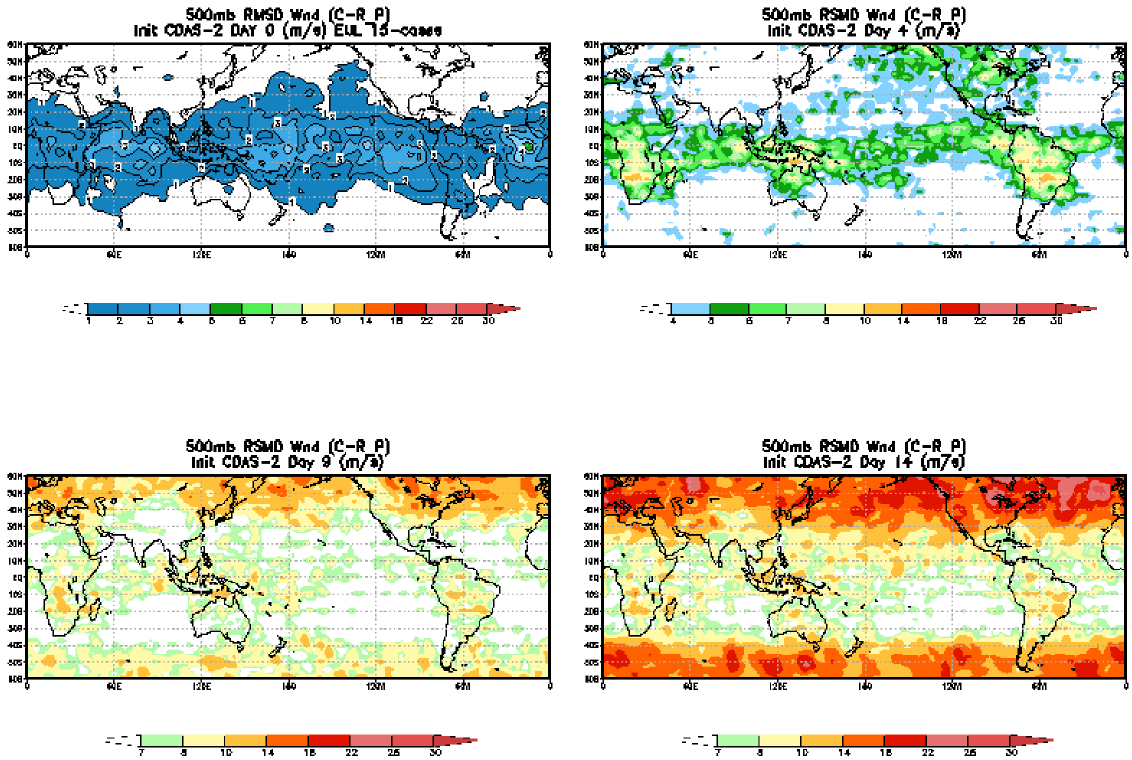

Fig. 7 RMS difference (m/s) as in Fig. 4 but for the Utah global Euler model.

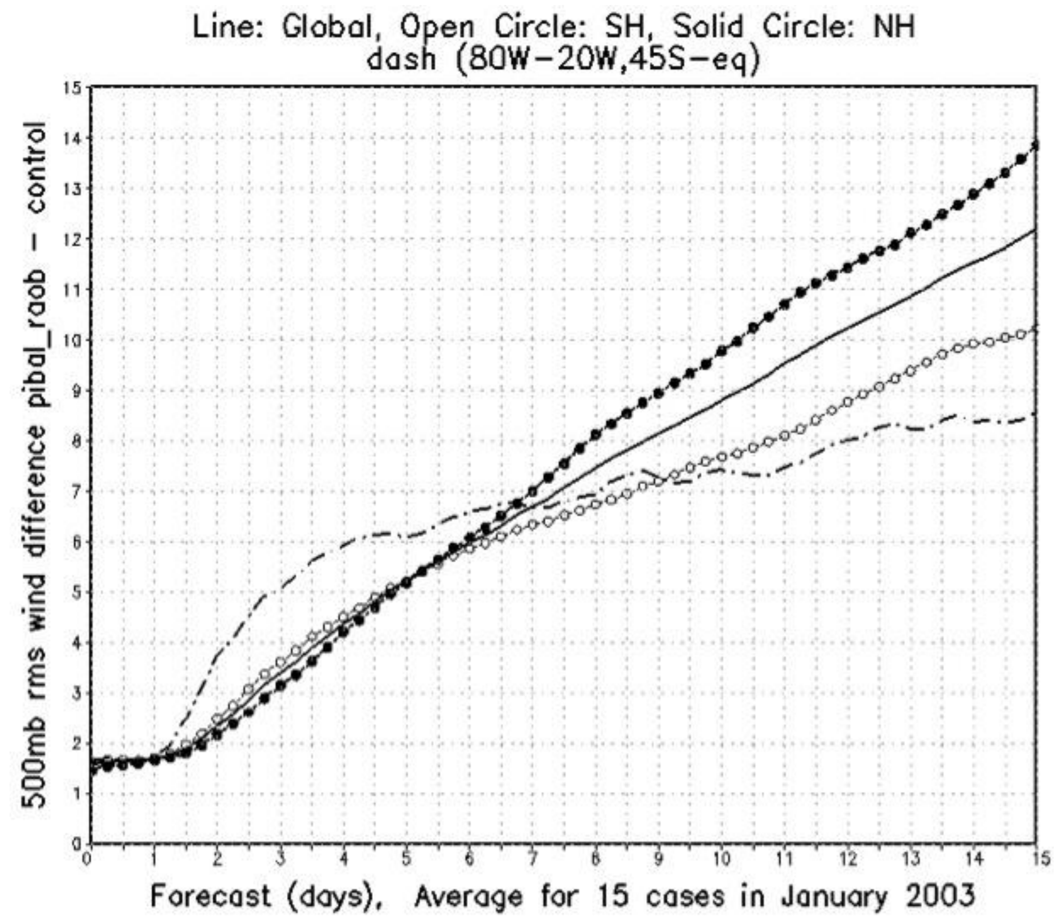

Fig. 8 Time evolution of area integrated rms sensitivity as in Fig. 5 but for the Utah global Euler model.

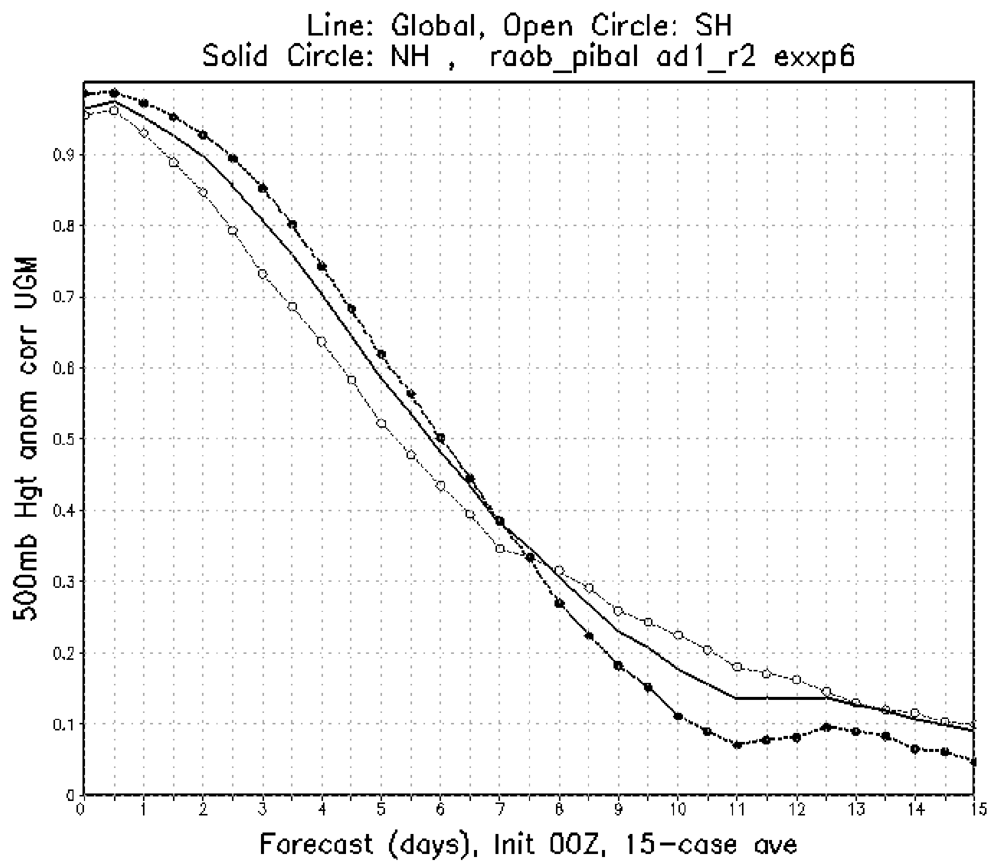

Fig. 9 Anomaly correlations of 500-mb geopotential height for Utah global primitive equations model (UGM) forecasts during January 2003 for the globe (solid line), Northern Hemisphere (solid circles), and Southern Hemisphere (open circles). CDAS-2 analyses containing SALLJEX data are used as verification. Climatology is 1951-2000 monthly climatology from the NCEP-NCAR Reanalysis, Version 1 (Kistler et al., 2001).

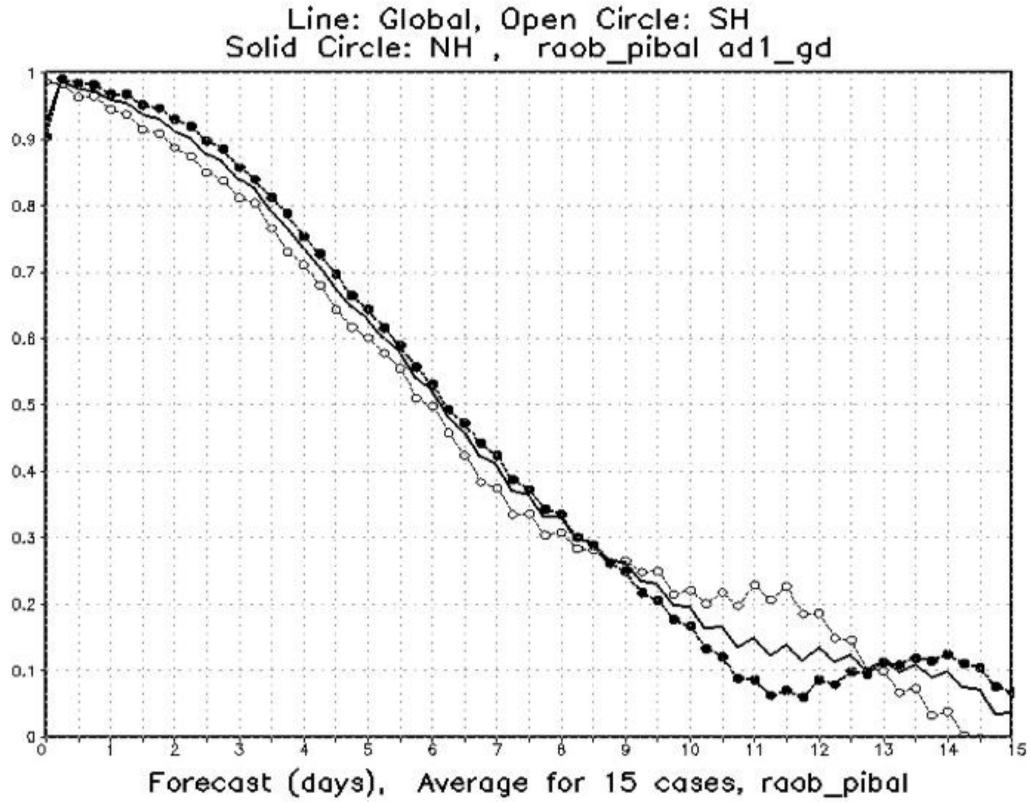

Fig. 10 Anomaly correlations of 500-mb geopotential height as in Fig. 9 but for the Utah Euler model forecasts.

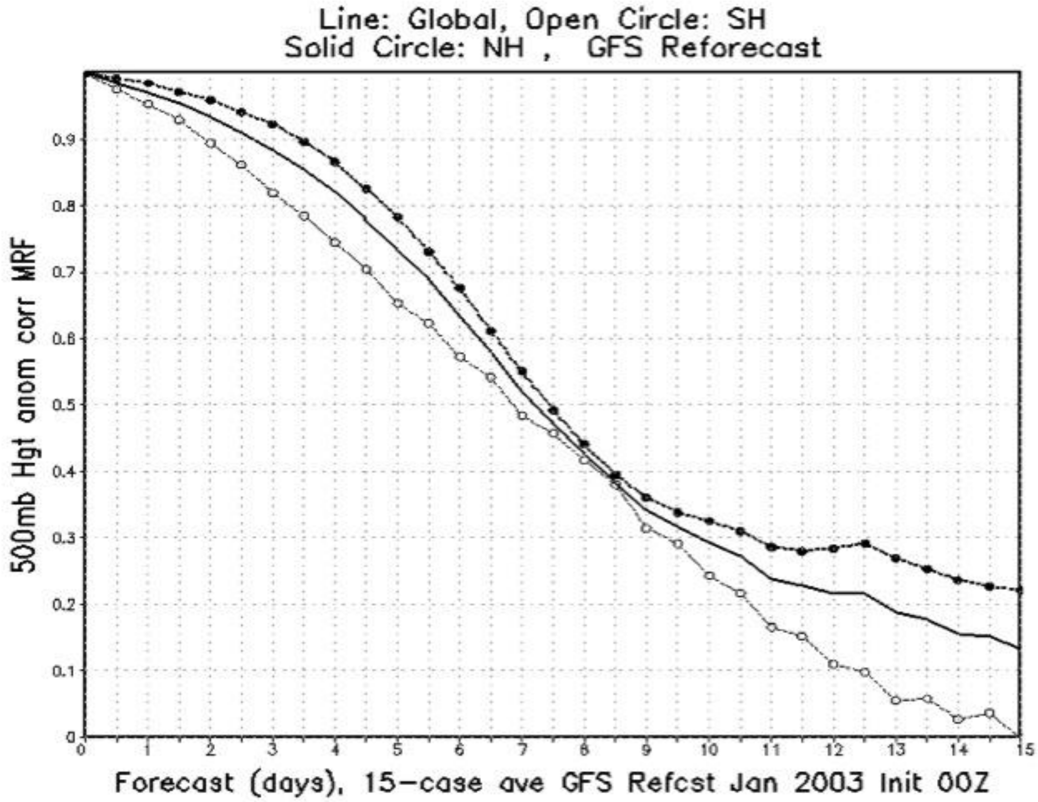

Fig. 11 Anomaly correlations of 500-mb geopotential height for the GFS reforecast ensemble average during January 2003 for the globe (solid line), Northern Hemisphere (solid circles), and Southern Hemisphere (open circles). CDAS-2 analyses containing SALLJEX data are used as verification. Climatology is 1951-2000 monthly climatology from the NCEP-NCAR Reanalysis, Version 1 (Kistler et al., 2001).

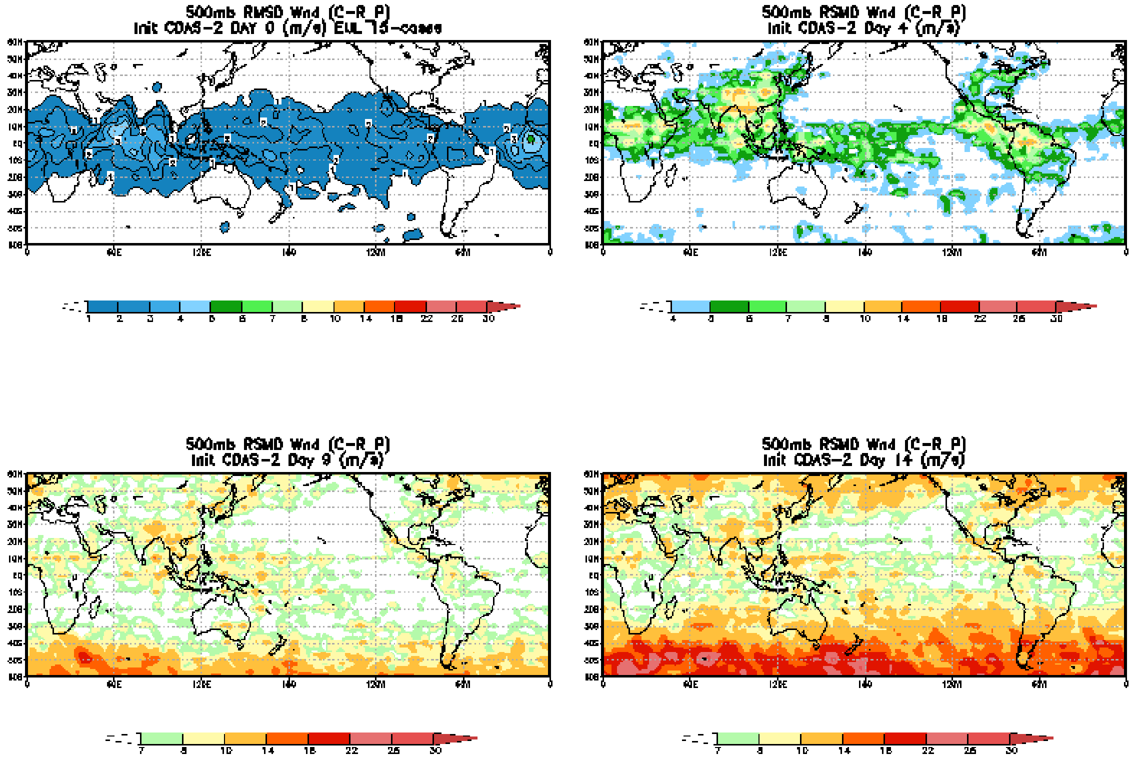

Fig. 12 RMS difference (m/s) between 500-mb wind forecasts made by the Utah global Euler model as in Fig. 7 but for the NAME experiment.

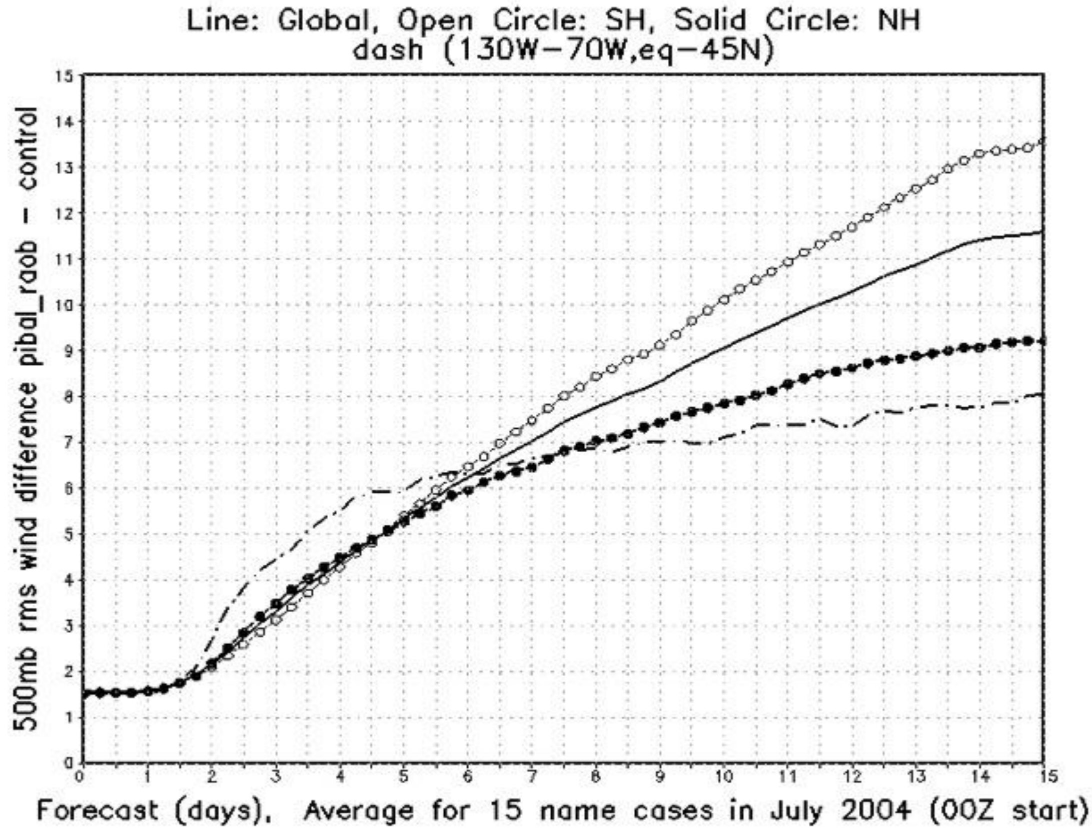

Fig. 13 Time evolution of area integrated rms sensitivity between 500-mb wind forecasts made by the Utah global Euler model as in Fig. 8 but for the NAME experiment initial states and global Euler forecasts using control initial states. The solid line represents globally-averaged sensitivity; solid circles Northern Hemisphere; open circles Southern Hemisphere; and the dashed line represents an average over a domain centered on the NAME region from 130W-70W, Eq-45N.

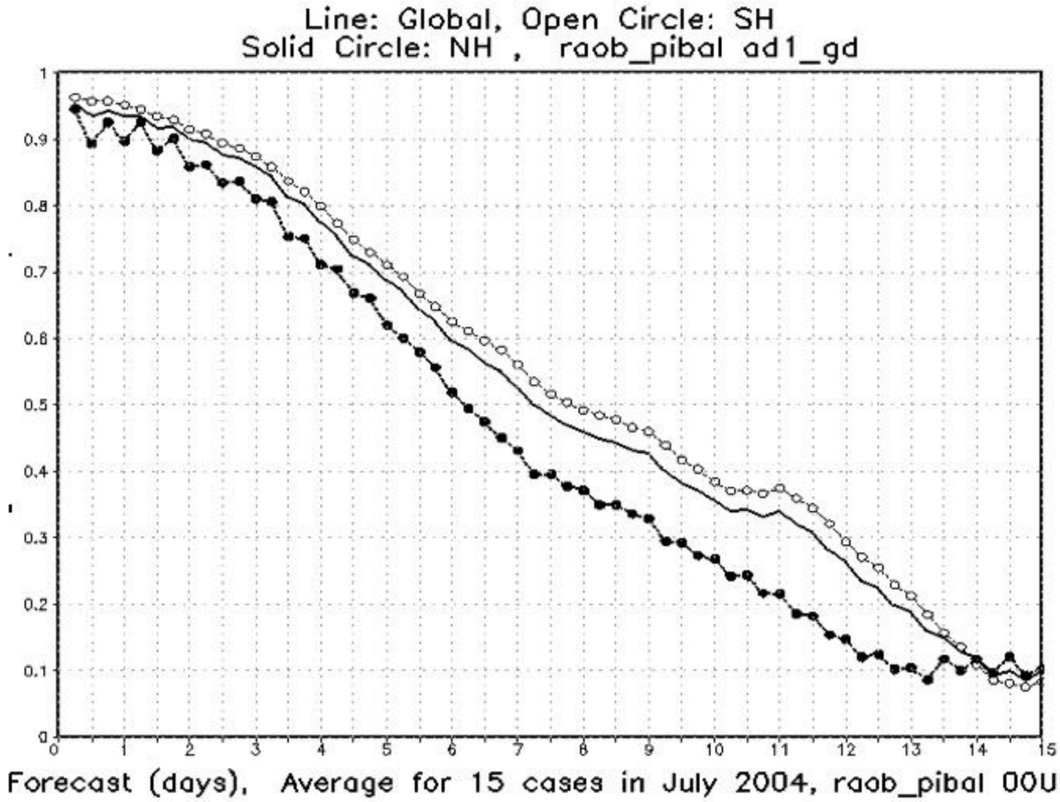

Fig. 14 Anomaly correlations of 500-mb geopotential height for Utah Euler model forecasts during July 2004 for the globe (solid line), Northern Hemisphere (solid circles), and Southern Hemisphere (open circles). CDAS-2 analyses containing NAME data are used as verification. Climatology is 1951-2000 monthly climatology from the NCEP-NCAR Reanalysis, Version 1 (Kistler et al., 2001).

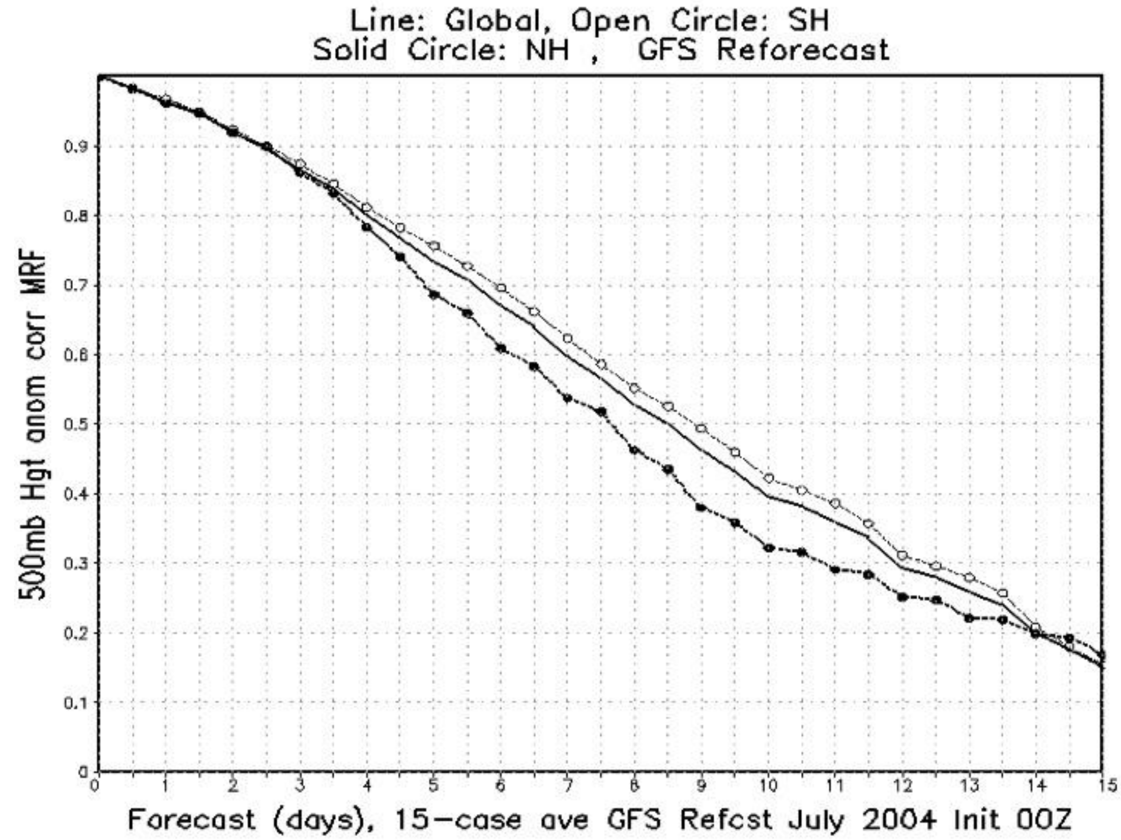

Fig. 15 Anomaly correlations of 500-mb geopotential height for the GFS reforecast ensemble average during July 2004 for the globe (solid line), Northern Hemisphere (solid circles), and Southern Hemisphere (open circles). CDAS-2 analyses containing NAME data are used as verification. Climatology is 1951-2000 monthly climatology from the NCEP-NCAR Reanalysis, Version 1 (Kistler et al., 2001).

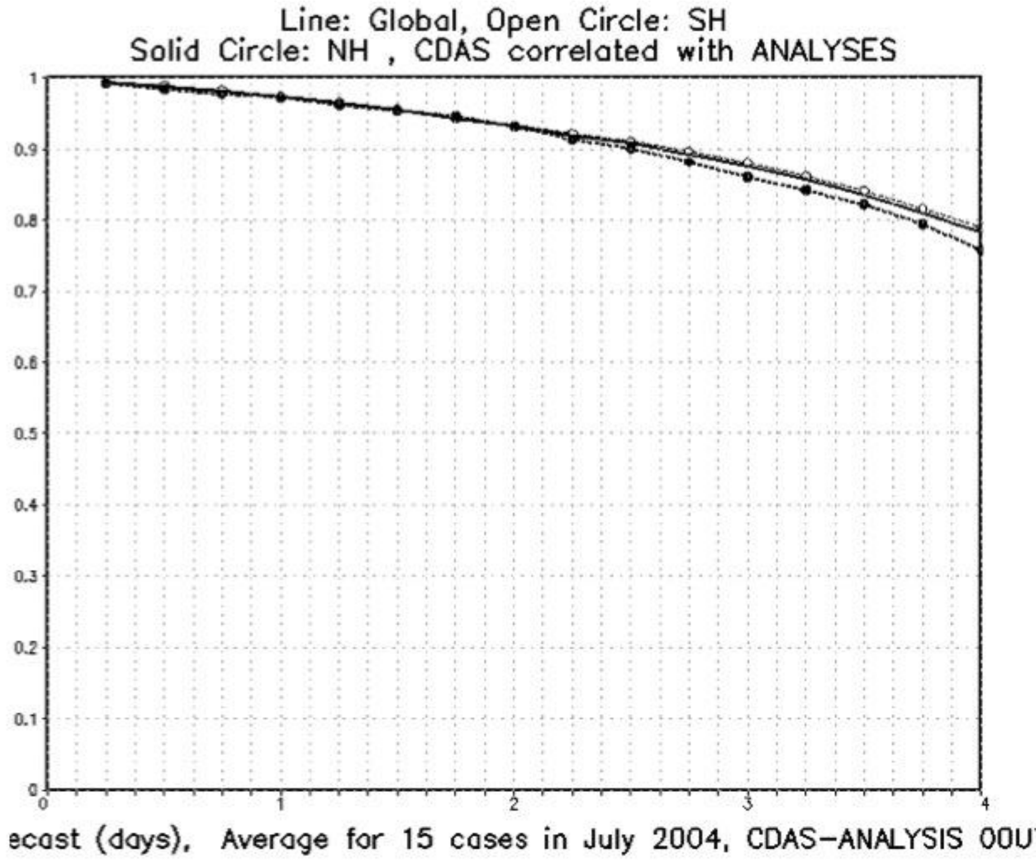

Fig. 16 Anomaly correlations of 500-mb geopotential height for the NCEP CDAS model (provided by Dr Kingtse Mo) during July 2004 for the globe (solid line), Northern Hemisphere (solid circles), and Southern Hemisphere (open circles). CDAS-2 analyses containing NAME data are used as verification. Climatology is 1951-2000 monthly climatology from the NCEP-NCAR Reanalysis, Version 1 (Kistler et al., 2001).

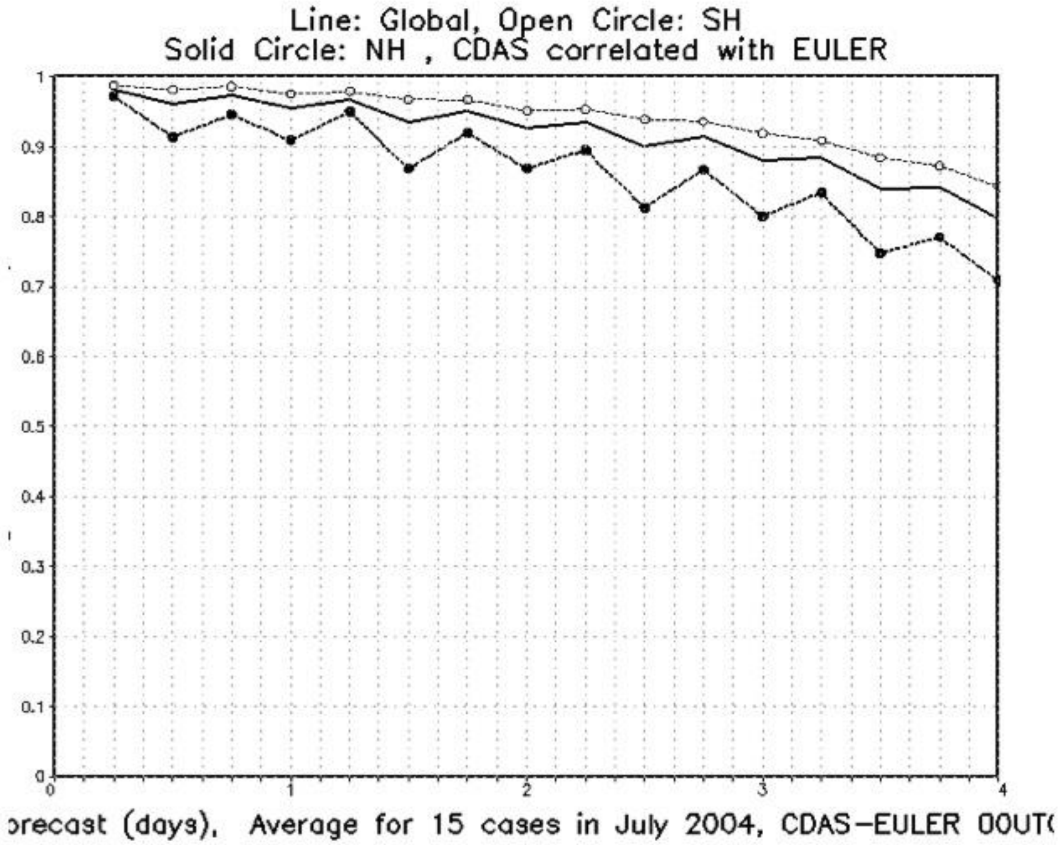

Fig. 17 As in Fig. 16, but for the Utah Euler model.

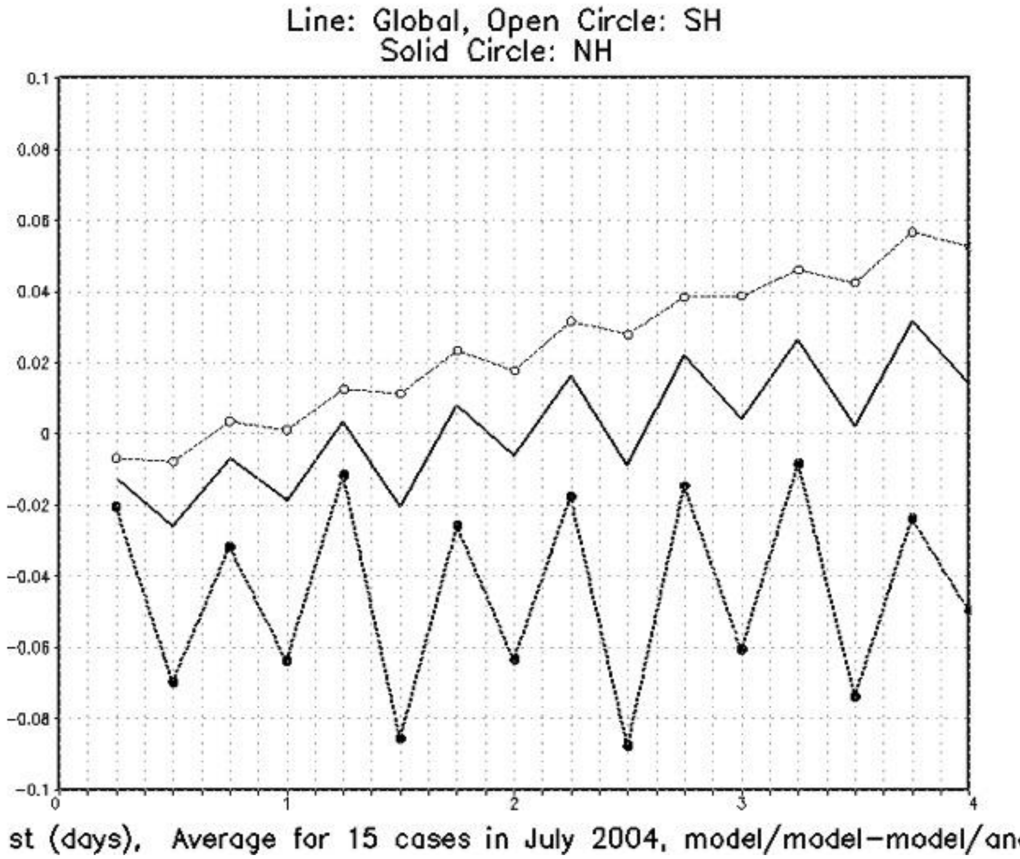

Fig. 18 The differences in anomaly correlations between the global Utah Euler and the CDAS model cases (i.e., values in Fig. 17 minus those of Fig. 16).

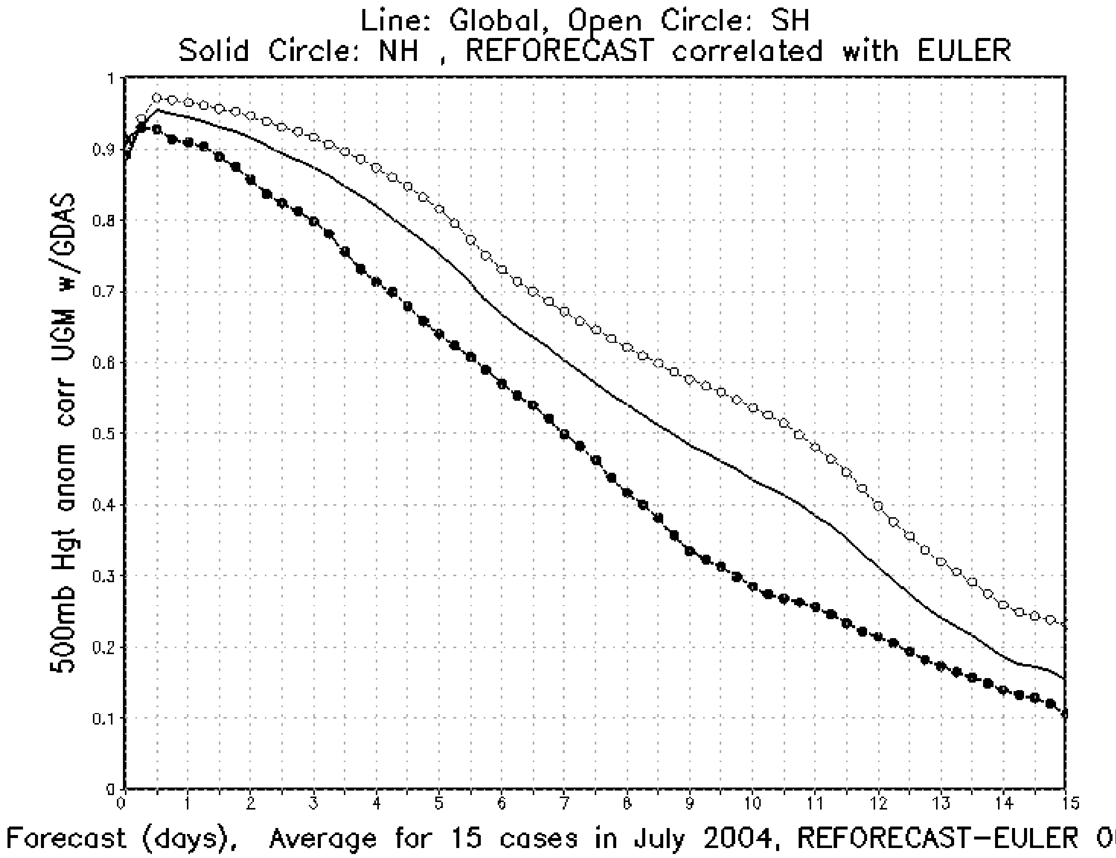

Fig. 19 Anomaly correlations of 500-mb geopotential height between the Utah Euler model and the GFS reforecasts during July 2004 for the globe (solid line), Northern Hemisphere (solid circles), and Southern Hemisphere (open circles). The curves illustrate how well the two models predict each other for the chosen cases. Climatology is 1951-2000 monthly climatology from the NCEP-NCAR Reanalysis, Version 1 (Kistler et al., 2001).

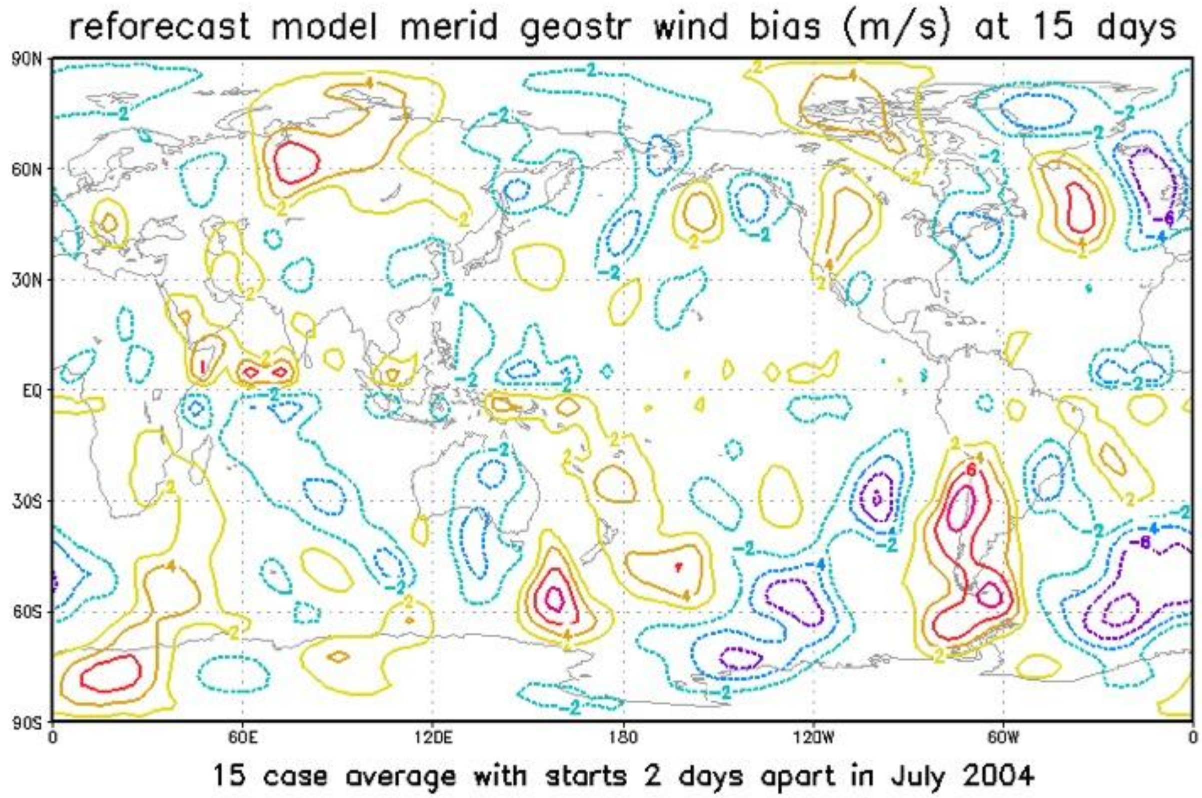

Fig. 20 The 15-case averaged 500-mb, meridional geostrophic wind biases (m/s) for 360 h (Day 15) predictions provided by the GFS reforecast ensemble average.

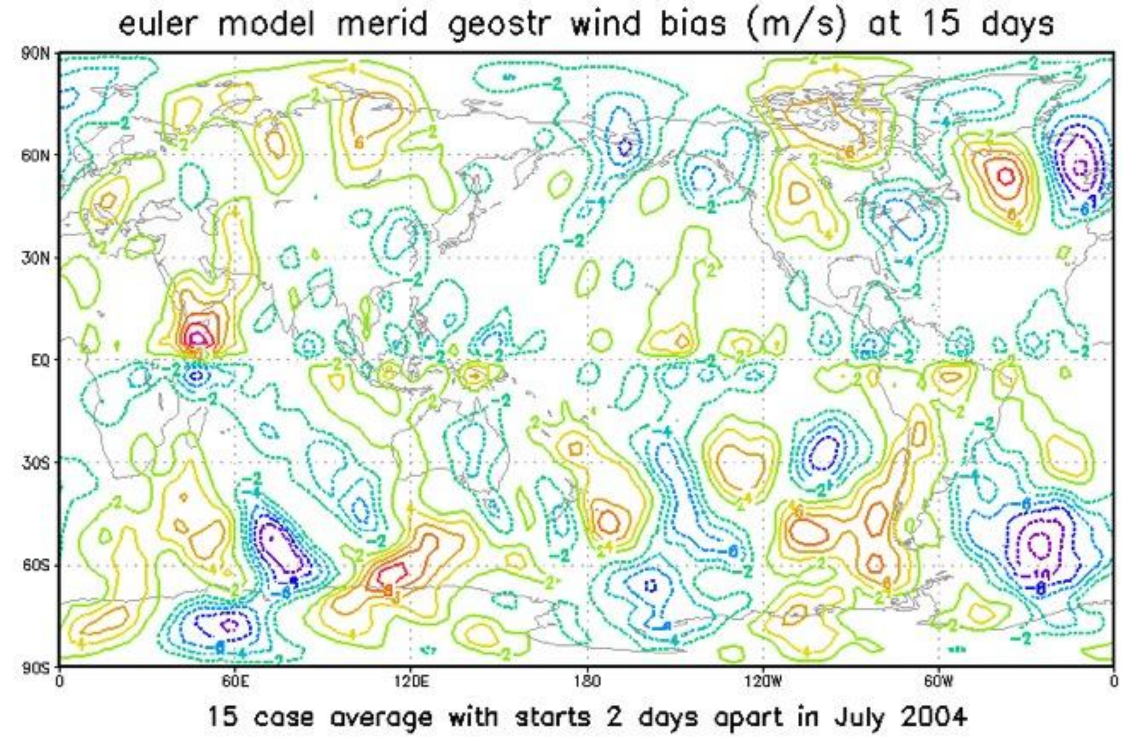

Fig. 21 The 15-case averaged 500-mb, meridional geostrophic wind biases (m/s) for 360 h (Day 15) predictions provided by the Utah Euler model.

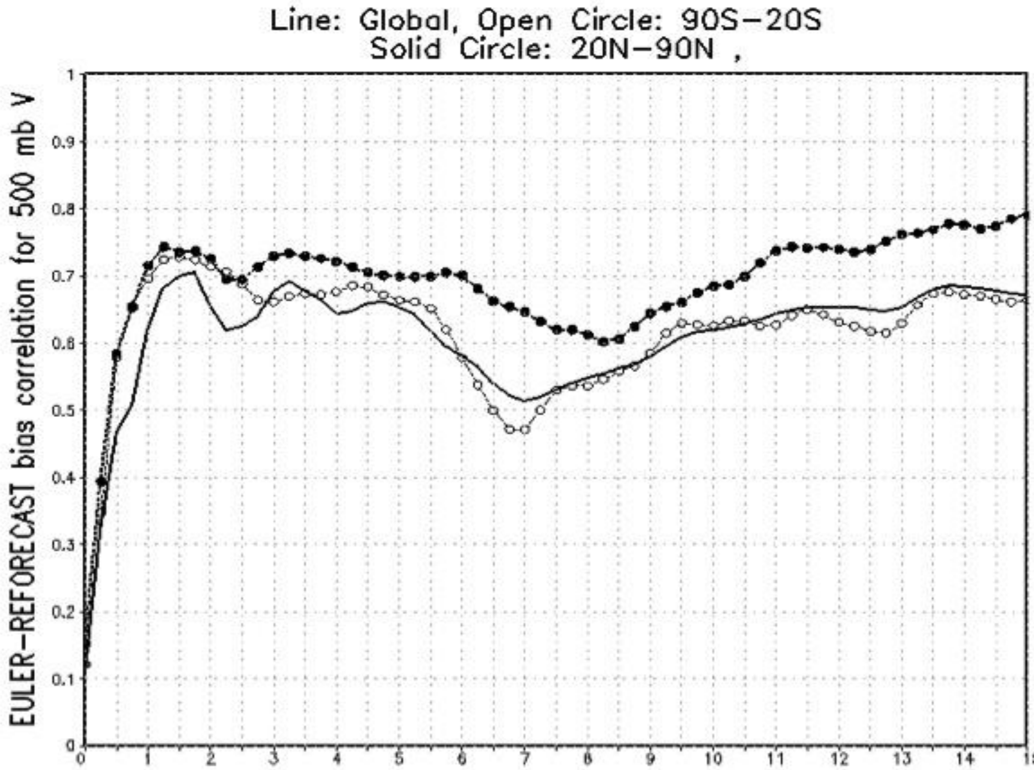

(Forecast Day →)

Fig. 22 Time evolution of correlations of meridional wind biases of the Euler model with meridional wind biases of the GFS reforecast model. Note how the bias correlations increase with forecast duration, and eventually exceed 0.5 globally and in each hemisphere.